Bioorganic & Medicinal Chemistry 18 (2010) 7365–7379

Contents lists available at ScienceDirect

Bioorganic & Medicinal Chemistry

journal homepage: www.elsevier.com/locate/bmc

Building a MCHR1 homology model provides insight into the receptor–antagonist contacts that are important for the development of new anti-obesity agents

Nuria Cirauqui [a], Anna K. Schrey [b], Silvia Galiano [a], Javier Ceras [a], Silvia Pérez-Silanes [a], Ignacio Aldana [a,*], Antonio Monge [a], Ronald Kühne [b,*]

[a] Unidad en Investigación y Desarrollo de Medicamentos, Centro de Investigación en Farmacobiología Aplicada (CIFA), Universidad de Navarra, C/Irunlarrea, s/n, 31080 Pamplona, Spain
[b] Leibniz-Institut für Molekulare Pharmakologie, Robert-Rössle-Str. 10, 13125 Berlin, Germany

ARTICLE INFO

Article history:
Received 4 April 2010
Revised 2 September 2010
Accepted 7 September 2010
Available online 15 September 2010

Keywords:
Melanin-concentrating hormone
Histamine 3 receptor
Antagonist
Molecular modeling
Obesity

ABSTRACT

Melanin-concentrating hormone (MCH) regulates feeding and energy homeostasis through interaction with its receptor, the melanin-concentrating receptor 1 (MCHR1), making it a target in the treatment of obesity. Molecular modeling and docking studies were performed in order to find a binding model for the docking of two new series of MCHR1 antagonists to the receptor. Results suggested interactions between the ligands and two glutamines (Gln5.42 and Gln6.55) not conserved in many of the GPCRs family members. Histamine 3 receptor (HRH3) presents two apolar residues in the aforementioned positions and the available biological data against this receptor supported the role of the two glutamines in the binding of antagonists to the MCHR1. This knowledge could be useful in the development of new, more active and more selective MCHR1 antagonists.

1. Introduction

Obesity has become an alarming public health problem worldwide. According to the World Health Organization, more than 1 billion adults are overweight (body mass index [BMI] >25), and among them, 300 million are truly obese (BMI >30).[1] Obesity is a major risk factor for many serious diseases including diabetes mellitus, hypertension, cardiovascular disease, and stroke.[2] Although the pathophysiology of obesity is not fully understood, it has been established that numerous receptors in the hypothalamus and other brain regions mediate satiety and food consumption.[3] These receptors are likely to become dysregulated upon chronic overfeeding and caloric imbalance;[4] returning them to normal function via small-molecule drugs is a potential strategy for obesity treatment.[5]

Melanin-concentrating hormone (MCH) is a 19-amino acid peptide predominantly expressed in the lateral hypothalamus and *zona incerta* areas of the brain.[6] A large number of experiments have been carried out and published regarding the role that MCH plays in obesity control. Intracerebroventricular injection of MCH induces feeding in rats.[7] Mice with an ablation of the MCH gene are hypophagic, hypermetabolic and lean,[8] while transgenic mice that overexpress MCH are hyperplasia, obese and show insulin resistance.[9] MCH acts through two G-protein-coupled receptors, melanin-concentrating receptor 1 (MCHR1) and melanin-concentrating receptor 2 (MCHR2). Physiological functions of MCHR2 are still unknown, but MCHR1 has been proved to be involved in feeding, metabolism regulation, and other functions, such as emotional behaviour.[10] Experiments showed that mice lacking MCHR1 are hyperactive, hypermetabolic and mildly hyperphagic.[11] Therefore, pharmacological blockade of MCHR1 appears as a promising approach for obesity treatment.

MCHR1 belongs to the 'brain-gut peptides receptor cluster', according to a chemogenomic analysis of the binding cavity of human GPCRs.[12] The cavity of this group of receptors is typically formed by two hydrophobic subsites; subsite 1 between transmembrane regions (TMs) 1, 2 and 7 and subsite 2 between TMs 5 and 6. At the center of the cavity, certain polar residues, such as Asp3.32(123) in MCHR1, connect both subsites.[12] There is experimental evidence of the binding of Asp3.32 to a basic amino nitrogen of the antagonist.[13,14] Several molecular modeling studies of the MCHR1 receptor have also suggested a hydrogen bond between residue Gln5.42(212) and a carbonyl group present in some antagonists.[15,16]

In this study, two novel series of MCHR1 antagonists have been used to develop a binding model to the receptor with the aim of

* Corresponding authors. Tel.: +34 948 425653; fax: +34 948 425652 (I.A.); tel.: +49 30 94793 229; fax: +49 30 94792 230 (R.K.).
E-mail addresses: ialdana@unav.es (I. Aldana), kuehne@fmp-berlin.de (R. Kühne).

0968-0896/$ - see front matter © 2010 Elsevier Ltd. All rights reserved.
doi:10.1016/j.bmc.2010.09.014

understanding the structure–activity relationships.[17] This process is hampered by the lack of experimentally derived structural data of MCHR1 and therefore, homology modeling is currently the only way to obtain a model of the antagonist/receptor complex. Most comparative modeling methods rely on sequence similarity to a structural template, from which the backbone structure is inherited. However, if this similarity is not close enough, both the backbone positioning and the side chain conformation play an important role and further information about ligand binding poses has to be incorporated into the process of modeling binding pockets. A ligand-steered approach, where existing antagonists are used to shape and optimize the binding site through a flexible-ligand–flexible-receptor docking, has already been used and thought to reduce the uncertainty in binding site modeling.[18]

2. Results and discussion

2.1. Selection of the GPCR template

Before 2007, the only eukaryotic GPCR X-ray structure available was that of the rhodopsin.[19] But in recent years the structural information available for GPCRs has rapidly increased. Two new opsin structures have been published,[20,21] as well as two β-adrenergic receptors,[22,23] and the adenosine receptor structures.[24]

For the construction of the homology model, the crystal structure of bovine rhodopsin (OPSD, protein data bank entry 1U19)[19] was selected as template. This structure was preferred over the other GPCR X-ray structures for different reasons. The new opsin structures were discarded because they represent active states of the receptor, while the binding of antagonists occurs in the inactive state.[20,21] Concerning Adenosin A2A receptor (AA2AR, pdb entry 3EML),[24] its TM3 does not appear to be important for the binding of antagonists,[24] while it has been proved by mutational studies that Asp3.32 in TM3 of MCHR1 is crucial for the binding of antagonists to our receptor.[13,14] Concerning the adrenergic receptors (ADRB2, pdb entry 2RH1;[22] ADRB1, pdb entry 2VT4),[23] a comparison of the ECL2 in OPSD, ADRB1, ADRB2 and MCHR1, suggested the use of rhodopsin as template. The ECL2 has already been reported to belong to the ligand binding pocket of GPCRs, and to be important for the binding of antagonists.[25] When comparing the Cα deviations of the ligand binding region (LBD) of the known GPCR X-ray structures (data not shown), we found that the main differences between the X-ray structures are located in the LBD part of ECL2. Looking at the alignment of the ECL2 residues for the OPSD, MCHR1, and ADRB2 receptors (ADRB1 is not shown for simplification, but coincides with ADRB2 in the points discussed here) (Fig. 1), three observations can be made with regard to this loop in the three proteins: (i) rhodopsin presents two cysteine residues in this loop, Cys110-Cys187, which form a disulfide bridge. On the contrary, in ADRB2, each of these cysteines is involved in a different interaction (Cys106-Cys191 and Cys184-Cys190). The MCHR1, similarly to rhodopsin, presents only two cysteine residues (Cys116 and Cys204), and therefore the disulfide bridge pattern in our receptor is expected to be that of the rhodopsin; (ii) the distribution of proline and glycine residues that disrupt an α-helical conformation is similar in the first two receptors, while none of these amino acids are found in ADRB2; (iii) the ECL2 in rhodopsin is stabilized by polar interactions involving residues Arg177 and His195. In contrast, the ECL2 in the ADRB2 is stabilized by hydrophobic interactions formed by several aromatic residues (Tyr174, Tyr185 and Phe193) which are not conserved in the other two receptors. Even though within the TM region MCHR1 has a higher sequence similarity to the adrenergic receptors in comparison to bovine rhodopsine, we believe that the expected spatial similarity of the ECL2 of MCHR1 compared with that of ADRB2 is the key argument for choosing the template.

2.2. Homology model building and docking studies

The applied methodology is summarized in Scheme 1. A homology model of MCHR1 based on the available crystal structure of bovine rhodopsin (OPSD, protein data bank entry 1U19)[19] was built followed by a minimization of the side chains (see Supplementary data for details on protein sequence alignment). In the first step, compound **2t** (Fig. 2), the most active of both series,[17] was docked in the receptor model using either the SURFLEX-DOCK program integrated in Sybyl v7.3,[26] or by applying the compound to a short molecular dynamics (MD) simulation (see Supplementary data for details). As a result, we selected three complex structures which were subjected to a restrained molecular dynamics simulation and further minimization in order to relax the side chains; these three complexes were then used as a starting point for repeated simulated annealing (SA) to sample different docking poses. From here, 14 models were selected according to the following criteria: (i) diversity of docking poses and interaction patterns and (ii) calculated interaction enthalpies of the ligand receptor complexes. Table 1 summarizes the various distance restraints applied in this simulated annealing procedure.

In the second step, the 35 compounds (Tables 2 and 3) were docked separately into each of the obtained receptor models using the SURFLEX-DOCK program integrated in Sybyl v7.3,[26] with a protomol constructed by ligand mode, and selecting the 10 best scored

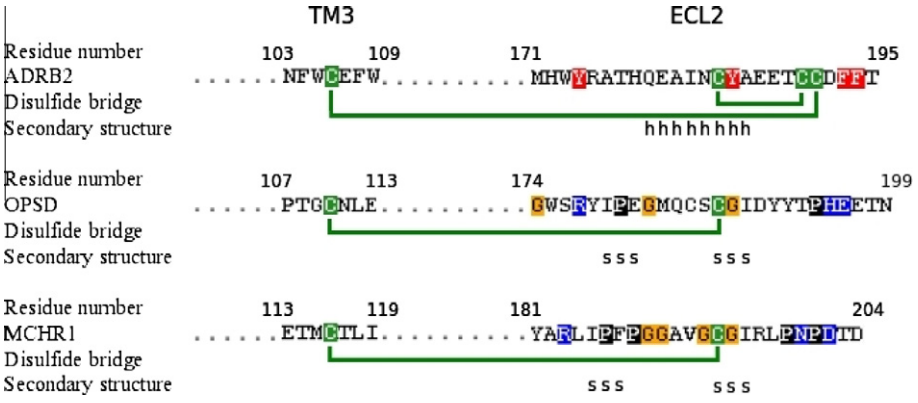

Figure 1. Sequence alignment of the residues of extracellular loop 2 for ADRB2, OPSD and MCHR1 receptors. In the secondary structure, 'h' stands for α-helix and 's' for β-strand. Polar residues stabilizing the ECL2 in OPSD and MCHR1 are shown in blue, while the aromatic ones that stabilize the ECL2 in ADRB2 are colored in red. Disulfide bridges involving residues of this loop are represented by green lines.

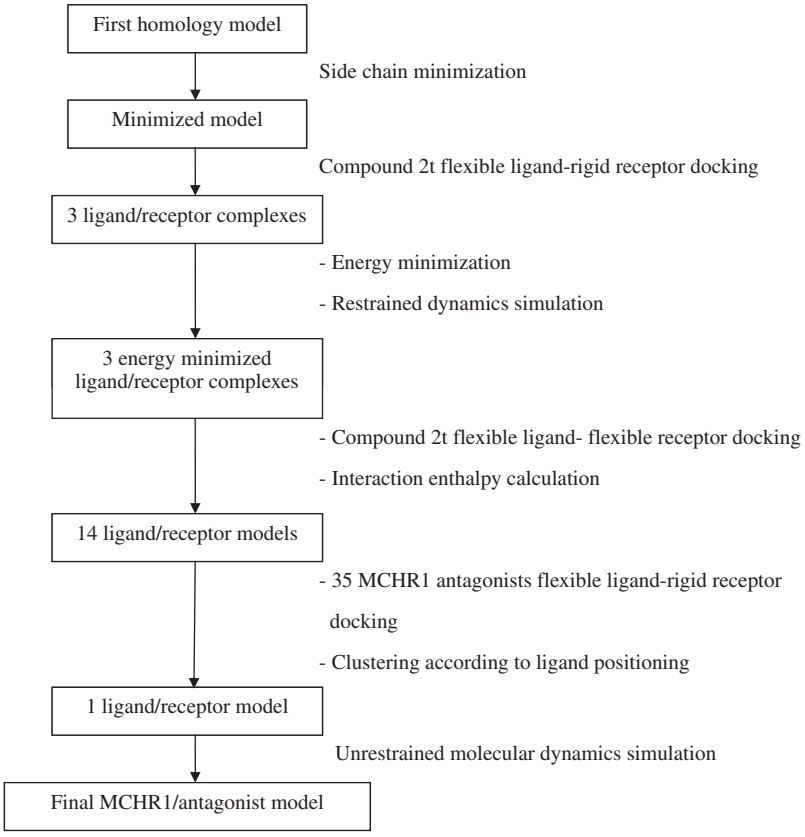

Scheme 1. MCHR1/antagonist model building method.

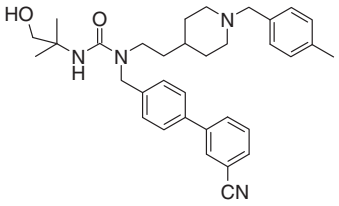

Compound 2t. K_i = 43 nM

Figure 2. Most active compound of MCHR1 antagonists series 1 and 2.[17]

docking poses. For each model, the 350 poses were sorted into groups according to their conformation and orientation in the receptor. From the whole study, the group that presented the best correlation between docking score and biological affinity data was selected as the preferred binding mode of the antagonists to the MCHR1.

This selected receptor/ligand complex (scaffold interactions shown in Fig. 3a) presented the following features: (i) the biphenyl group was located among residues Phe5.47(217), Phe5.51(221) and Tyr6.52(273); (ii) the *p*-toluyl moiety was located in subsite 1, between residues Phe187(ECL2) and Tyr7.43(301); (iii) an ionic interaction between Asp3.32(123) and the basic amine of the antagonist was found;[13,14] (iv) Gln5.42(212) formed a hydrogen bond to the hydroxyl group of the ligand; (vi) Tyr6.52(273) formed a hydrogen bond to the urea hydrogen atom; and (vi) Thr3.40(131) formed a hydrogen bond to the cyano group.

Table 1
Summary of all the distance restraints used during the different simulated annealing runs

Domain	Residues and/or antagonist scaffolds	Comment	Ref.
TM1-antagonist	Phe1.39(47), Pro1.58(97) *p*-toluyl ring of antagonist	Binding of the *p*-toluyl ring in hydrophobic subsite 1 (TMs 1, 2 and 7)	12
TM2–TM4[a]	Asn2.45(84)-Trp4.41(168)	Hydrogen bond found in the inactive state of rhodopsin	33
TM3[a]	Arg3.50(140)-Asp3.51(141)	Salt bridge characteristic of the inactive state of GPCRs (E/DRY motif)	33,34
TM3[a]	Asp3.32(123)	Orientation of Asp3.32 relative to antagonist binding	47
TM3-antagonist[a]	Asp3.32(123) basic amine of the antagonist	Salt bridge found by molecular substitution and mutational experiments in GPCRs	13,14
TM5-antagonist	Gln5.42(212) carbonyl group of the antagonist	Molecular modeling studies for binding of antagonist to the MCHR1	15,16
TM5/TM7-antagonist	Thr5.39(209), Gln5.42(212), Gln6.55(276) hydroxyl group of the antagonist	Different positioning of the hydroxyl group attempted	—
TM6[a]	Trp6.48(269)-Phe6.44(265)	Hydrophobic interaction characteristic of the inactive state of rhodopsin	19,23
TM6[a]	Trp6.48(269)-Tyr6.51(272)	Hydrophobic interaction characteristic of the inactive state of rhodopsin	19,23
TM6	Tyr6.51(273)	Rotation of the aromatic ring inside the receptor, relative to its potential role in receptor activation	48–50
TM7	Tyr7.35(293)	Orientation thought for the inactive state of GPCRs	50

[a] Restraints applied in all the runs.

Table 2
Binding affinities of compounds **1a–j** (series 1) towards MCHR1 and HRH3 receptors

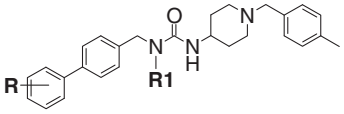

Compound	R1	R	K_i[a] (nM) (pK_i ± SEM[b]) MCHR1	K_i[c] (nM) ± SEM[b] HRH3	Selectivity MCHR1/HRH3[d]
1a	H	4-F	545 (6.265 ± 0.145) (n = 2)	nd	nd
1b	H	4-OMe	1460 (5.84) (n = 1)	5150 ± 2130 (n = 2)	3.53
1c	H	2-OMe	425 (6.37 ± 0.03) (n = 2)	>10^3 (n = 3)	MCHR1
1d	H	3-CN	186 (6.73 ± 0.15) (n = 2)	>10^3 (n = 4)	MCHR1
1e	H	–H	2640 (5.575 ± 0.055) (n = 2)	>10^3 (n = 2)	MCHR1
1f	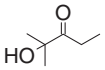	4-F	5860 (5.23 ± 0.06) (n = 2)	1420 ± 15 (n = 2)	0.242
1g	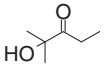	4-OMe	>10^3	581 ± 76 (n = 3)	HRH3
1h	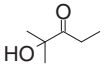	2-OMe	6050 (5.22) (n = 1)	9990 ± 721 (n = 2)	1.65
1i	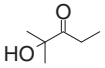	3-CN	6380 (5.195 ± 0.075) (n = 2)	2800 ± 385 (n = 2)	0.438
1j	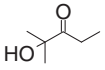	–H	>10^3	>10^3 (n = 2)	nd

[a] MCHR1(h)/[3H]SNAP-7941/HEK/SPA-BF136-1. K_i is the in vitro inhibition constant.
[b] Standard error of the media.
[c] HRH3/[^{125}I]Iodoproxyfan. K_i is the in vitro inhibition constant.
[d] 'MCHR1' and 'HRH3' stand for compounds that are selective for MCHR1 and HRH3, respectively. Compounds were considered to have no affinity to the receptor if K_i >10^3 nM.

Table 3
Binding affinities of compounds **2a–z** (series 2) towards MCHR1 and HRH3 receptors

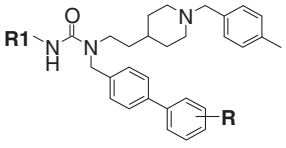

Compound	R1	R	K_i[a] (nM) (pK_i ± SEM[b]) MCHR1	K_i[c] (nM) ± SEM[b] HRH3	Selectivity MCHR1/HRH3[d]
2a		4-F	314 (6.505 ± 0.155) (n = 2)	nd	nd
2b		4-OMe	273 (6.56 ± 0.13) (n = 3)	6510 ± 485 (n = 2)	23.8
2c		2-OMe	>10^3	>10^3 (n = 2)	nd
2d		3-CN	509 (6.29 ± 0.12) (n = 2)	853 ± 252 (n = 3)	1.68
2e		–H	258 (6.59 ± 0.84) (n = 3)	>10^3 (n = 2)	MCHR1
2f	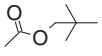	4-F	421 (6.375 ± 0.175) (n = 2)	2080 (n = 1)	4.94
2g	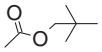	4-OMe	595 (6.225 ± 0.125) (n = 2)	1010 ± 220 (n = 3)	1.70
2h	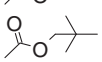	2-OMe	215 (6.668 ± 0.135) (n = 4)	1050 ± 246 (n = 2)	4.88
2i	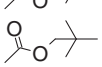	3-CN	254 (6.595 ± 0.055) (n = 2)	1630 ± 677 (n = 3)	6.42
2j	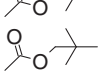	–H	947 (6.02 ± 0.14) (n = 2)	1130 (n = 1)	1.19
2k	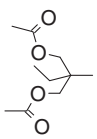	4-F	214 (6.67 ± 0.05) (n = 2)	548 ± 18 (n = 2)	2.56

Table 3 (*continued*)

Compound	R1	R	K_i[a] (nM) (pK_i ± SEM[b]) MCHR1	K_i[c] (nM) ± SEM[b] HRH3	Selectivity MCHR1/HRH3[d]
2l	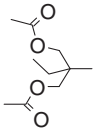	4-OMe	170 (6.77 ± 0.01) (*n* = 2)	779 ± 173 (*n* = 3)	4.58
2m	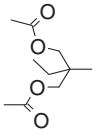	2-OMe	1200	629 ± 95 (*n* = 2)	0.524
2n	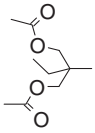	3-CN	1080	1310 ± 370 (*n* = 2)	1.21
2o	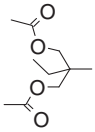	–H	388 (6.41 ± 0.03) (*n* = 2)	807 ± 110 (*n* = 2)	2.08
2p		4-F	96.6 (7.015 ± 0.135) (*n* = 2)	>10^3	MCHR1
2r		4-OMe	204 (6.69) (*n* = 1)	9260 ± 339 (*n* = 4)	45.4
2s		2-OMe	251 (6.6 ± 0.04) (*n* = 2)	6680 ± 921 (*n* = 5)	26.6
2t		3-CN	43 (7.36 ± 0.01) (*n* = 2)	1160 ± 25 (*n* = 2)	26.9
2u		–H	144 (6.84 ± 0.015) (*n* = 2)	nd	nd
2v		4-F	149 (6.825 ± 0.145) (*n* = 2)	>10^3	MCHR1
2w		4-OMe	143 (6.84 ± 0.12) (*n* = 3)	899 ± 15 (*n* = 2)	6.29
2x		2-OMe	167 (6.78 ± 0.1) (*n* = 2)	2140 ± 545 (*n* = 3)	12.8
2y		3-CN	769 (6.11 ± 0.04) (*n* = 2)	8800 ± 140 (*n* = 2)	11.4
2z		–H	173 (6.76 ± 0.01) (*n* = 2)	nd	nd

[a] MCHR1(h)/[3H]SNAP-7941/HEK/SPA-BF136-1. K_i is the in vitro inhibition constant.
[b] Standard error of the media.
[c] HRH3/[^{125}I]Iodoproxyfan. K_i is the in vitro inhibition constant.
[d] 'MCHR1' and 'HRH3' stand for compounds selective for MCHR1 and HRH3, respectively. Compounds were considered to have no affinity to the receptor if K_i >10^3 nM.

2.3. Model validation by molecular dynamics simulations

As a criterion for the accuracy of the selected ligand–receptor model, the stability of the complex was tested by an unrestrained 2 ns molecular dynamics simulation using a previously described setup.[27] The conformation closest to the average one in the production run was selected as our final MCHR1/antagonist model.

Table 4 shows the root mean square deviation (RMSD) of the transmembrane domains and the residues in the binding site (those showing interactions with the ligand, Fig. 3a) for the average structure compared to the bovine rhodopsin and the β-2-adrenergic receptor (ADRB2, protein data bank entry 2RH1).[19,22] All values are within the X-ray structure resolutions (2.2 Å for OPSD and 2.4 Å for ADRB2). As can be observed, even if the rhodopsin structure is used as template, the final complex model, particularly in the binding site, shows low deviation compared to all of the other receptors.

Figure 4 presents the average fluctuation of the α-carbons in the production phase (last 760 ps of the trajectory). In general, the transmembrane regions have a low RMSD, while the loops show much greater flexibility. There are, however, some exceptions: (i) extracellular loop 2 (ECL2) remains more rigid than the other loops during the simulation, (ii) some parts of the transmembrane domains show a higher fluctuation, as in the case of the extracellular ends of TMs1-5; and (iii) the cytoplasmatic region of TM4.

Concerning the ECL2, the antiparallel β-strand of this loop in the rhodopsin X-ray structure, that we had hypothesized for the

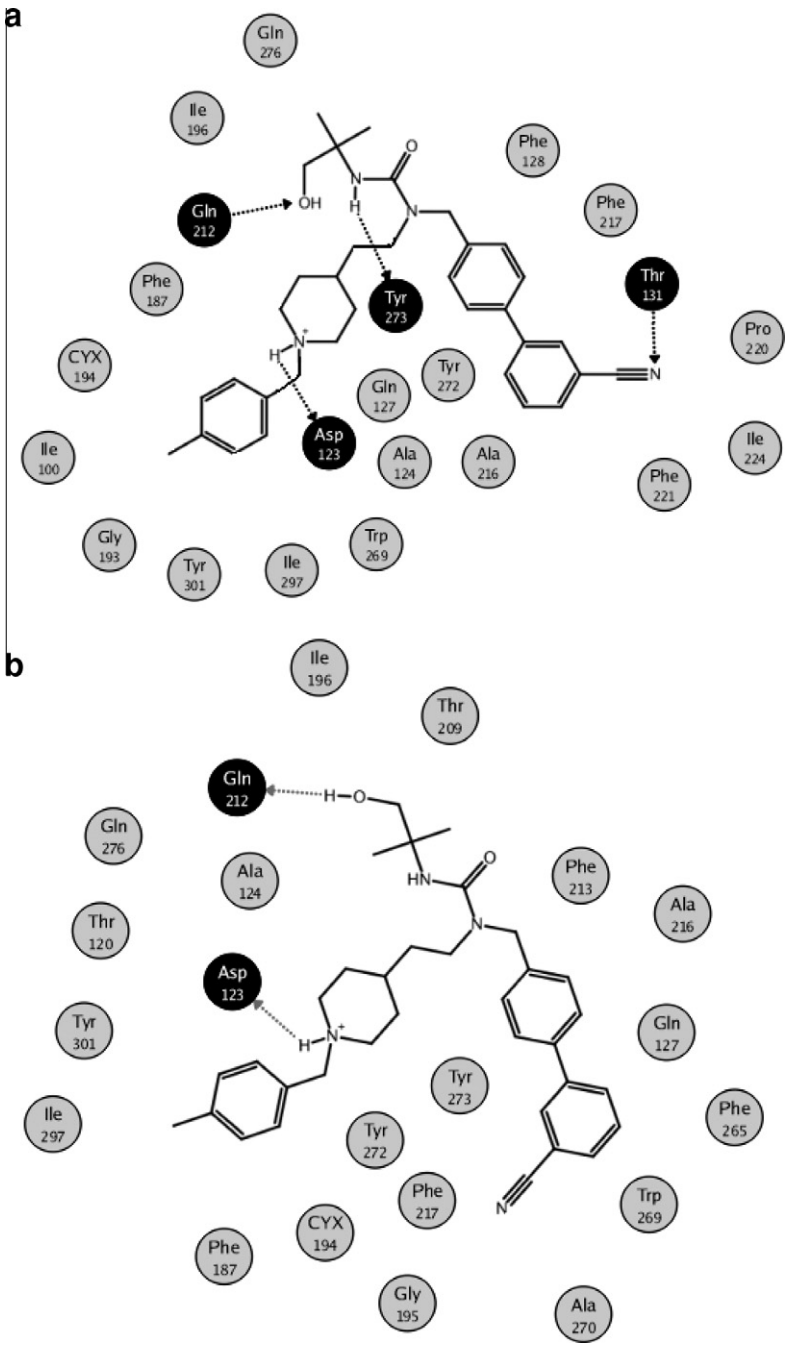

Figure 3. 2D diagram of the ligand–receptor interactions found in the selected MCHR1/antagonist model before (a) and after (b) the molecular dynamics simulation. Residues that form a hydrogen bond to the antagonist are stressed in black, and the hydrogen bonds are shown by arrows. Figures were generated with the software MOE.[51]

MCHR1 (see 'Structural template election'), remains stable during the whole simulation, conferring the observed rigidity. Moreover, this structural motive had been predicted for the MCHR1 by the secondary structure predictor SAM-TO2,[28] and it has also been suggested for other GPCRs.[29,30] In addition, looking at the structure of this loop in the rhodopsin and ADRB2 X-ray structures and in our MCHR1 model (Fig. 5), two observations come up which coincide with the proposed β-strand: (i) the disulfide bridge present in our model (Cys116-Cys204) coincides with that of rhodopsin (Cys110-Cys187), but is different in ADRB2 and (ii) the ECL2 stabilization pattern in rhodopsin (polar interactions involving residues Arg177 and His195) is also conserved in MCHR1 (Arg183, Asn200), while it is not present in ADRB2 (hydrophobic interactions formed by aromatic residues not conserved in the other two receptors). All these observations together support the proposed β-strand conformation in the extracellular loop 2 of MCHR1.

Table 4
Root mean square deviation (RMSD) in Ångström for the backbone heavy atoms of the final MCHR1 model compared to the OPSD (pdb entry 1U19) and ADRB2 (pdb entry 2RH1) X-ray structures

	RMSD MCHR1/ OPSD	RMSD MCHR1/ ADRB2	RMSD OPSD/ ADRB2
Transmembrane domains	2.2684	2.6361	2.1719
Binding site	1.4159	1.6630	1.3642

With regard to the transmembrane domains, ADRB2 and MCHR1 are characterized by a bigger cavity between the extracellular ends of the α-helices compared to OPSD (Fig. 6a), caused by

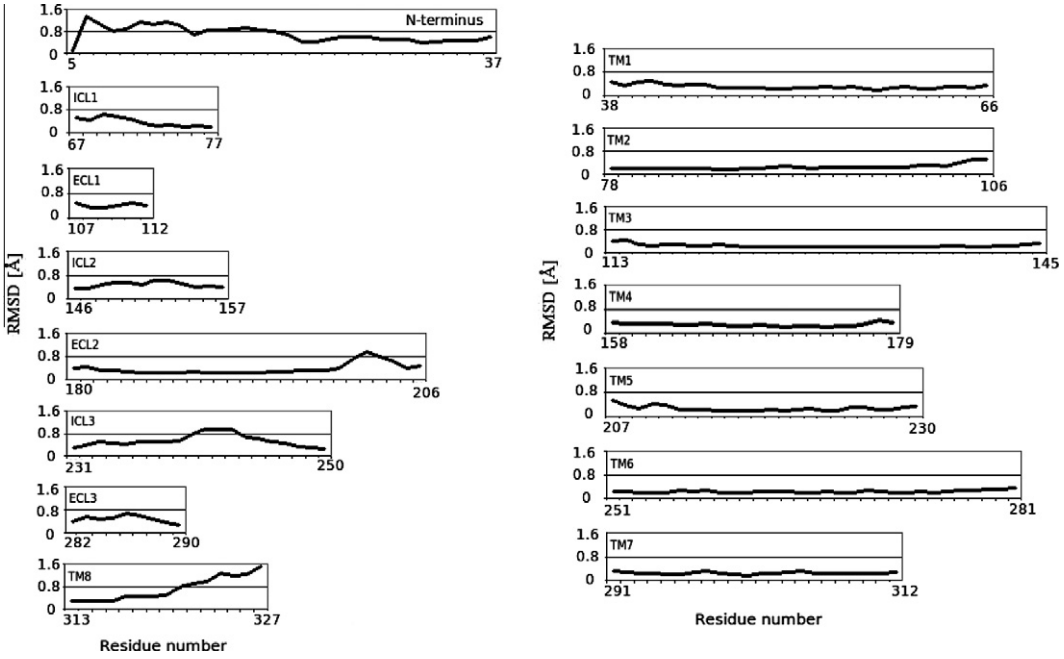

Figure 4. Root mean square deviation (RMSD) of the α-carbons of both transmembrane helices and loops in the production phase of the molecular dynamics simulation.

tilts of TM1 in ADRB2, TM2 in MCHR1 model and TM3 in both receptors. This could explain the increased flexibility of MCHR1 in these regions and may possibly be related to the fact that these receptors, in contrast to rhodopsin, are activated by ligands coming from the extracellular side.

On the other hand, the cytoplasmic regions are more stable and present a more similar shape in all three structures (Fig. 6b), except for the last residues in TM4 (Ser4.40(158) and Val4.41(159)) that have higher RMSD. These positions are occupied in rhodopsin by an asparagine and a histidine, which form a hydrogen bond. In MCHR1, the lack of this interaction could confer higher elasticity in this region.

2.4. Inspection of the inactive GPCRs structural features

Antagonists bind to receptors in their inactive state, maintaining them in that state. The inactive conformation of the structural template used (OPSD)[19] must then be observed in our final model, after the binding of the antagonist. Therefore, the structural features typical of the inactive state of GPCRs were inspected, looking for their presence in the final model, as well as determining their degree of stability during the whole simulation. With regard to Trp6.48(269), it interacts with both Phe6.44(265) and Tyr6.51(272), and is oriented towards a polar residue in position 7.45 (Asn303 in MCHR1), similar to that found in rhodopsin structures.[19,31] Another important conserved element is the E/DRY motif, which is supposed to hold together the cytoplasmic ends of TM3 and TM6 in the resting state.[32] Figure 7 shows a picture of this motif in the OPSD, MCHR1 and ADRB2 receptors. In rhodopsin, Arg3.50 forms a network of interactions with Glu3.49, Glu6.30 and Thr6.34. The MCHR1 presents a threonine in position 6.30 and the interaction of this residue with Arg3.50 was not observed in our study, nor was it found in other molecular modeling studies concerning this receptor.[15] The lack of this interaction could be explained by the shorter length of the threonine's side chain compared to that of glutamine. This weakening in the E/DRY motif is also observed in the ADRB2 receptor crystal structure, which presents a leucine in position 6.34. Moreover, the ADRB2 receptor lacks the interaction between Arg3.50 and Glu6.30. This could be an artefact of the crystallization procedure, which uses T4 lysozime to stabilize TMs5 and 6. But it could also be explained by the fact that ADRB2 presents a threonine in position 3.49, and not a glutamine as the rhodopsin receptor. The shorter length of the threonine's side chain could force Arg3.50 to move closer to TM3 and therefore farther from Glu6.30. The consequences of this weakening of the E/DRY motif in the MCHR1 and ADRB2 structures are patent in Figure 6b. A greater distance can be observed between the intracellular ends of TMs 3 and 6 in these two receptors compared to rhodopsin, due to tilts in TM3 in the ADRB2 receptor and TM6 in both receptors. Another structural feature found in the inactive state of GPCRs is the NPxxY motif. In this motif, the side chains of Asn7.49 and Tyr7.53 project inside the receptor, holding TM2 and TM7 together by means of a pair of interactions: Tyr7.53-Asn2.40 and Asn7.49-Asp2.50.[33] Figure 8 shows images of these interactions in the rhodopsin receptor, the ADRB2 and the MCHR1 model. In the β2-adrenergic receptor crystal structure, the first interaction is absent and the side chain of Tyr7.53 points towards Asn7.49. Both conformations were found during our molecular dynamics simulation and, even though the one similar to ADRB2 was more frequent, our final model presents the rhodopsin's pattern, with a hydrogen bond between Tyr7.53 and Asp2.40. Other interactions between conserved residues that stabilize the resting state and were found in our model include Asn1.50-Asp2.50 and Asn2.45-Trp4.50 (see Fig. 9).[33]

2.5. Analysis of the proposed binding mode

Most of the receptor–ligand contacts present in the first MCHR1/antagonist complex were maintained during the simulation (Fig. 3b), except for the interaction between residue Tyr6.52(273) and the urea hydrogen atom; and that between Thr3.40(131) and the cyano group. On the other hand, some aromatic residues located near the biphenyl scaffold oriented their side chains to create an aromatic cage for the binding of this group.

The binding pocket cavity obtained is typical of the 'brain gut receptor cluster':[12] two hydrophobic subsites (subsite one among TMs 1, 2 and 7, and subsite two between TMs 5 and 6) separated by a polar residue (Asp3.32). Figure 10 shows a 3D image of the

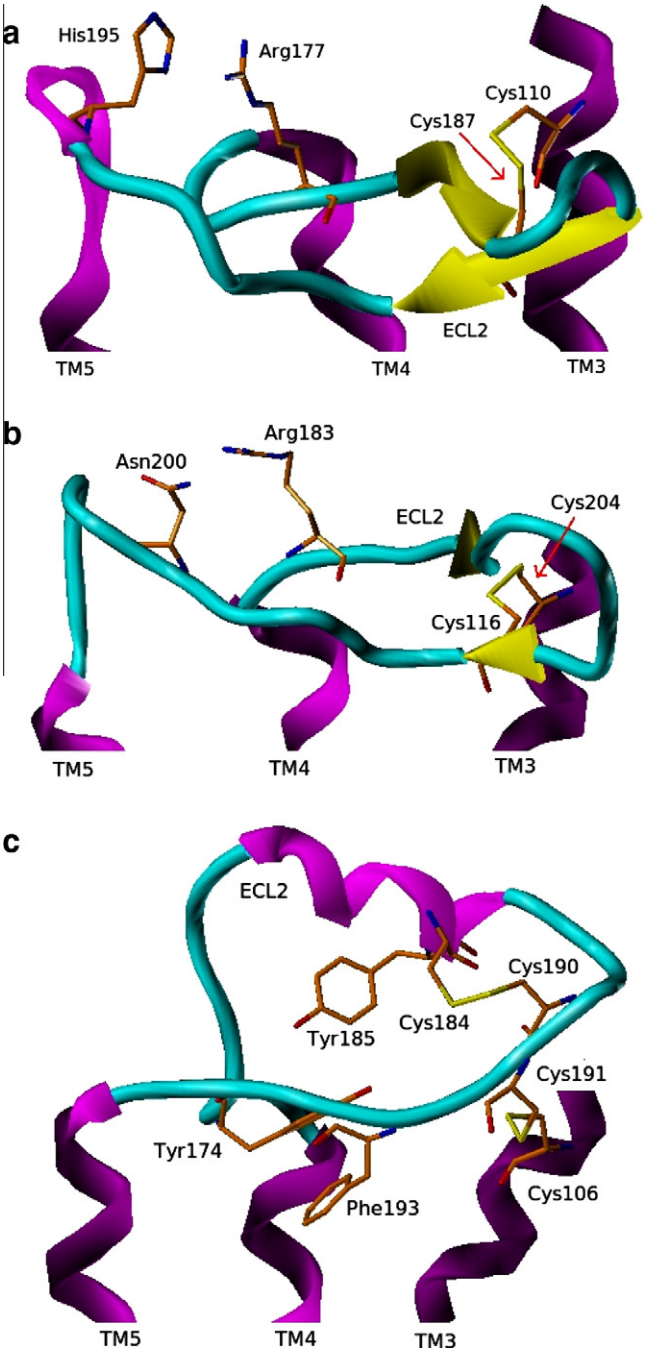

Figure 5. Structure of the extracellular loop 2 (ECL2) of OPSD (a),[19] MCHR1 (b) and ADRB2 (c)[22] receptors. Carbon atoms are colored orange, oxygen atoms are in red, nitrogen atoms are in blue and sulfur atoms are in yellow. Figures were generated with Sybyl v7.3.[26]

binding pose. Coinciding with the experimental findings, a salt bridge was found between Asp3.32(123) and the basic amine of the antagonist.[13,14]

In the eastern part of the molecule, the *p*-toluyl group binds into subsite 1 surrounded by residues Met2.57(96), Ile3.28(119), Tyr6.51(272), Ile7.39(297) and Tyr7.43(301). Most of them are common binding residues in this GPCR cluster.[12,18] Mutagenesis studies have shown Tyr6.51 and Tyr7.43 to be important for the binding of antagonists to the neurotensin-1-receptor, which also belongs to this group of receptors.[34] Other molecular modeling studies with MCHR1 propose hydrophobic interactions between Ile7.39(297) and the antagonist *T-226296*.[15] In our model, the *p*-toluyl ring of the ligand is also involved in π stacking interactions with Phe187 (ECL2). A role for the ECL2 in the binding of antagonists to MCHR1 had already been suggested by a molecular modeling study performed by Taveres et al., who found interactions between their antagonist and residues Pro188 and Val192 in the ECL2.[35]

As previously mentioned, the biphenyl moiety binds in an aromatic cage formed by residues Phe5.43(213), Phe5.47(217), Phe6.44(265), Phe6.45(266), Trp6.48(269) and Tyr6.52(273). This location coincides with experimental and computational findings regarding both the 'brain gut receptor cluster' and the 'amines receptor cluster'.[16,18,36–38]

The *N*-alkyl substituent R1 binds in a pocket between Gln5.42(212), Thr5.39(209) and Gln6.55(276). The hydroxyl group of the ligand forms a hydrogen bond with the side chain of Gln5.42 that remains stable during the whole simulation. Other molecular modeling studies have also proposed a role for Gln5.42 in the binding of antagonists to MCHR1, finding an interaction between this residue an a carbonyl group present in their antagonists (*T-226296* or *2-(2, 4-dichlorophenoxy)-N-{2-[(2-dimethylaminoethyl)methylamino]-4-methylquinolin-6-yl}-acetamide*).[15,16]

Moreover, Gln3.36(127) has been reported to contribute to the binding site.[11,18,39,40] In our model, Gln3.36(127) is close to the biphenyl moiety and the distance between the polar groups of our antagonist and this residue does not permit an interaction. The same was observed in a molecular modeling study conducted by Giordanetto et al., who found some of their antagonists bound too far from Gln3.36(127) so as to allow an interaction with it.[40] However, in our model, Gln3.36(127) is involved in a network of hydrogen bonds Tyr6.52(273)-Gln3.36(127)-Asp3.32(123)-Tyr7.43(301) which, together with the network of interactions Tyr6.51(272)-Gln6.55 (276)-Tyr7.35(293), were formed during the molecular dynamics simulation, contributing to the stability of the binding pocket. Therefore, Gln3.36(127) contributes to the binding site described here.

2.6. Structure–activity study

The docking pose of series 2 compounds is illustrated with compound **2t** in Figures 3b and 10. Due to the differences in structure between series 1 and 2, we present Figure 11, a structural model of compound 1e docked in the receptor, as an illustrative example of docking pose of series 1 compounds.

In vitro MCHR1 binding data for series 1 and 2 are given in Tables 2 and 3, respectively. In general, compounds from series 1 display lower affinity than those of series 2, probably due to the higher rigidity of the linker between amine and biphenyl groups in the first series. There is also a strong difference between compounds **1a–e** and compounds **1f–j**. In the first group, a hydrogen atom of the urea interacts with residue Gln5.42(212). In our model, substitutions in this position (**1f–j**) yield steric clashes with the glutamine and other residues lining the binding pocket.

In series 2, higher affinity for the receptor is shown for compounds **2p–z**, which present a hydroxyl group that interacts with Gln5.42(212). Furthermore, in compounds **2v–z**, a second hydroxyl group is predicted to be bound to Gln6.55(276). Even when presenting two polar interactions with different glutamine residues, compounds **2v–z** did not show better affinities than compounds **2p–u**, probably due to the higher steric hindrance of their R1 chain.

On the aromatic region, the electrostatic properties of the aromatic system could play an important role, and the different influence could be explained by both polar interactions with some residues, and electron-donating and withdrawing effects of substituents on the biphenyl system, which are not fully captured by the docking model. Also, the location of the biphenyl group inside the aromatic cage is important. Bigger substituents on the urea (R1 chain) could obligate the biphenyl group deeper into the pocket.

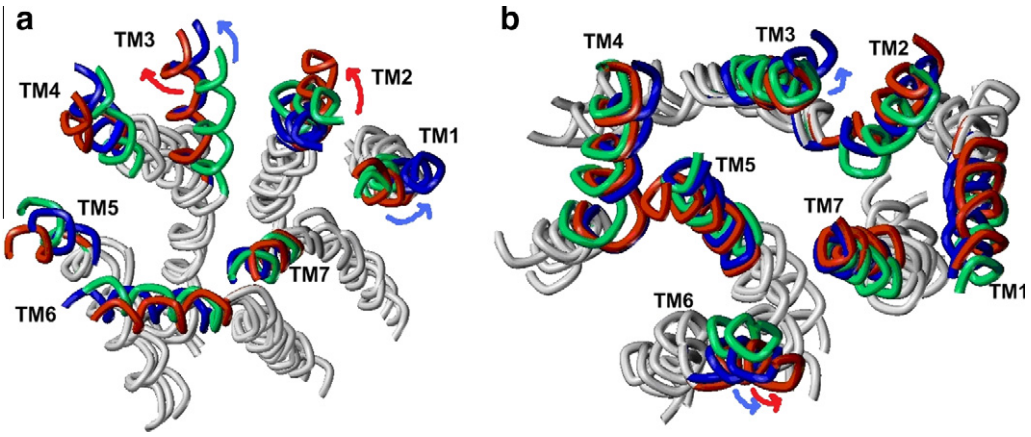

Figure 6. Alignment of OPSD (green)[19] and ADRB2 (blue)[22] X-ray structures with the final MCHR1 model (red). View from the extracellular (a) and intracellular (b) sides. A bigger cavity between the extracellular ends of the transmembrane domains is observed in ADRB2 and MCHR1 compared to the OPSD, caused by tilts of TM1 in ADRB2, TM2 in MCHR1 and TM3 in both receptors. With regard to the intracellular side, the distance between TM3 and TM6 in both ADRB2 and MCHR1 receptors is higher than in OPSD, due to the lack of certain interactions within the EDRY motif. Figures were generated with Sybyl v7.3.[26]

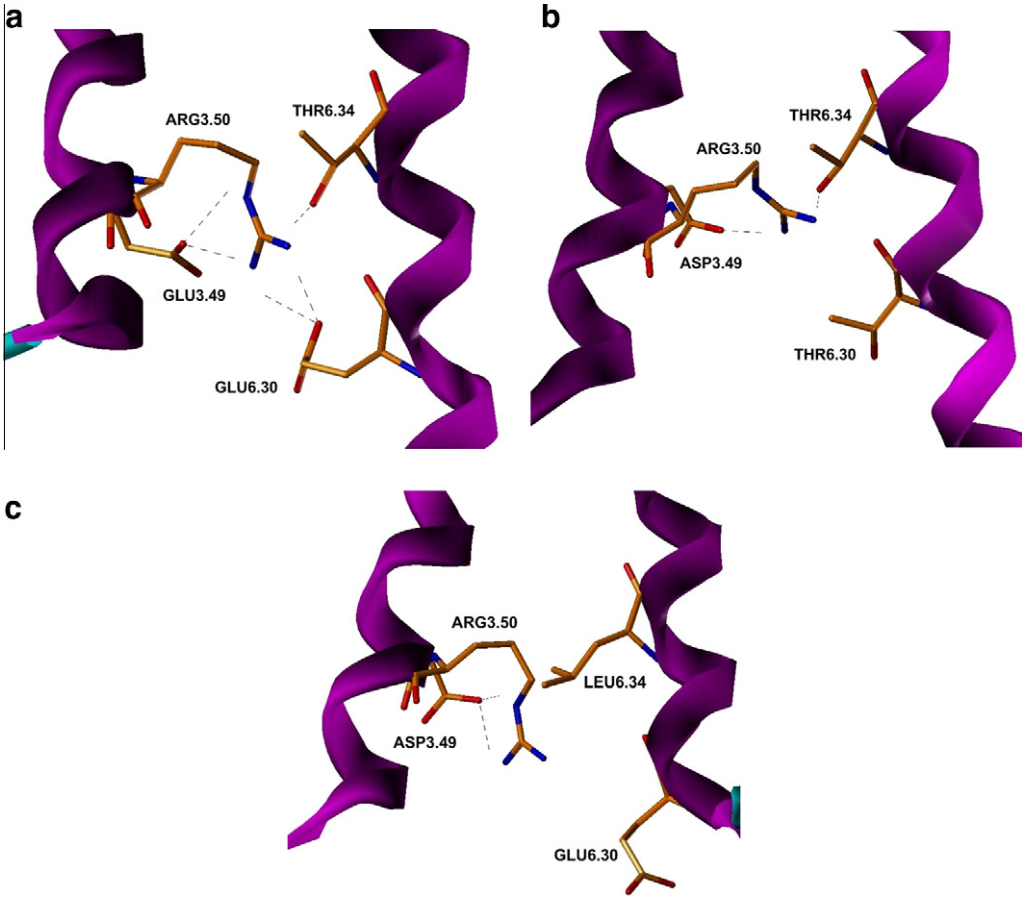

Figure 7. Interactions within the E/DRY motif observed in the OPSD (a)[19] and ADRB2 (b)[22] crystal structures, and in the MCHR1 (c) final model. Carbon atoms are colored orange, oxygen atoms are in red and nitrogen atoms are in blue. Atomic interactions within hydrogen bond distance are shown as dashed black lines. Figures were generated with Sybyl v7.3.[26]

This would modify the interactions of the aromatic scaffold with the different residues within the aromatic cage.

2.7. Model validation using biological affinity data against HRH3 receptor

Unfortunately, we could not carry out a mutational study to prove the role of Gln5.42 and Gln6.55, so we had to look for a different approach. Biological affinity data of the compounds against HRH3 was already available, so we decided to use it as a test to check the importance of the aforementioned glutamine residues in the binding to MCHR1. Our approximation is based on three arguments: (i) homology between HRH3 and MCHR1 within the binding site residues, (ii) similarity of the proposed binding mode of antagonists to HRH3 compared with that proposed by our model, (iii) and mainly the fact that HRH3 presents two

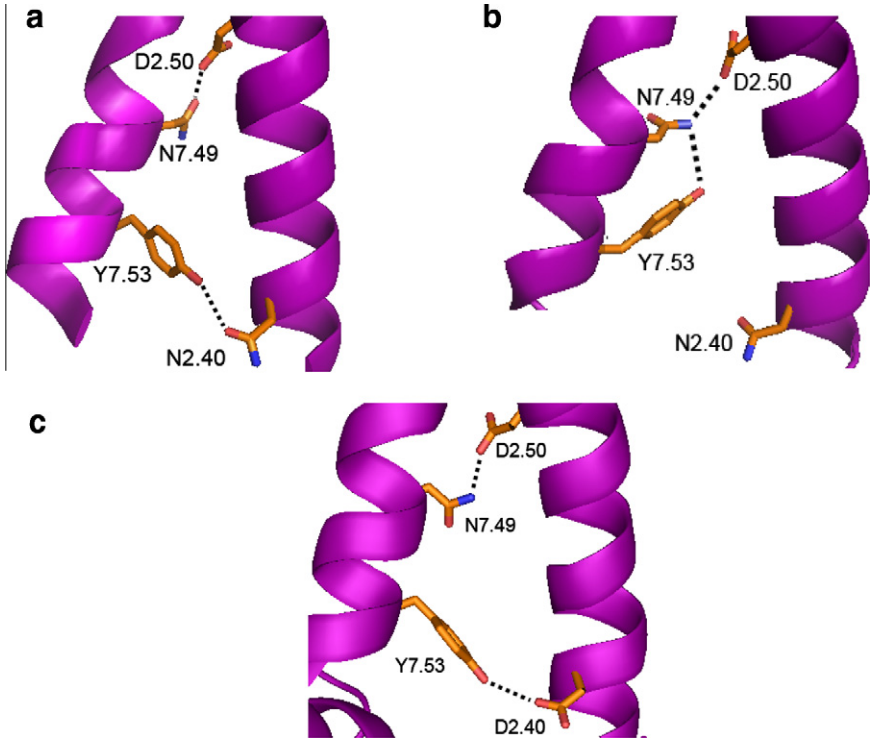

Figure 8. Interactions within the NPxxY motif observed in the OPSD (a)[19] and ADRB2 (b)[22] crystal structures, and in the MCHR1 (c) final model. Carbon atoms are colored orange, oxygen atoms are in red and nitrogen atoms are in blue. Atomic interactions within hydrogen bond distance are shown as dashed black lines. Figures were generated with Pymol (DeLano Scintific, Palo Alto, CA, USA).

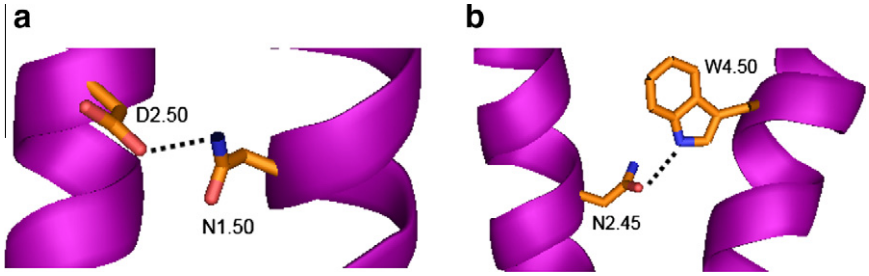

Figure 9. Other stabilizing interactions of the resting state of GPCRs found in our MCHR1 final model. Hydrogen bonds between Asn1.50 and Asp2.50 (a) and between Asn2.45 and Trp4.50 (b). Carbon atoms are colored orange, oxygen atoms are in red and nitrogen atoms are in blue. Atomic interactions within hydrogen bond distance are shown as dashed black lines. Figures were generated with Pymol (DeLano Scintific, Palo Alto, CA, USA).

apolar residues (Ala5.42 and Met6.55) instead of the glutamines (Fig. 12).

The homology between both receptors in the binding site was studied by an alignment of 30 hotspot residues supposed (from the X-ray structure of rhodopsin bound to retinal) to line the TM binding cavity of GPCRs (Fig. 12).[12] The receptors have a 23.3% of sequence identity within the binding site, which is comparable to that found between MCHR1 and either ADRB2 (30%), ADRB1 (26.6%), AA2AR (20%) or OPSD (20%). The binding site residues similarity between MCHR1 and other receptors of its same GPCR receptor cluster (with the exception of MCHR2) is also not higher (16.6–33.3%). Moreover, the residues found in this study to constitute the aromatic cage for the binding of the biphenyl group of our antagonists are conserved between MCHR1 and HRH3 in a percentage of 71.4%.

Concerning the binding mode of antagonists, HRH3 is thought to present a cavity formed by two hydrophobic subsites: subsite 1 between TMs 1, 2 and 7 (with mainly aliphatic residues) and subsite 2 between TMs 5 and 6 (with a strong aromatic character). Asp3.32 connects both subsites.[12] The same was found for MCHR1 in our model, as described above. Moreover, Lorenzi et al. showed that the aromatic moieties of classical HRH3 antagonists preferentially bind in an aromatic cage between TM3, TM6 and TM7.[41] The location of that aromatic cage is similar to that found for MCHR1 antagonists in our model, with the difference that in our model, the aromatic was cage displaced toward TM5.

Finally, the lack of the two glutamine residues in the HRH3 receptor allows us to check the importance of those residues in the binding to MCHR1.

In vitro HRH3 binding data for series 1 and 2 are given in Tables 2 and 3, respectively. As expected, in general, the affinity of the compounds to this second receptor did not differ much from that to the MCHR1. However, some compounds were found to be selective to our receptor. This is the case for antagonists **1a–e**, whose urea NH-group was proposed by our model to interact with Gln5.42 (Ala in HRH3). In contrast, compounds **1f–j**, whose *N*-alkyl chain clashes with the side chain of Gln5.42 in our model, show improved affinity against HRH3. Moreover, in series 2, higher

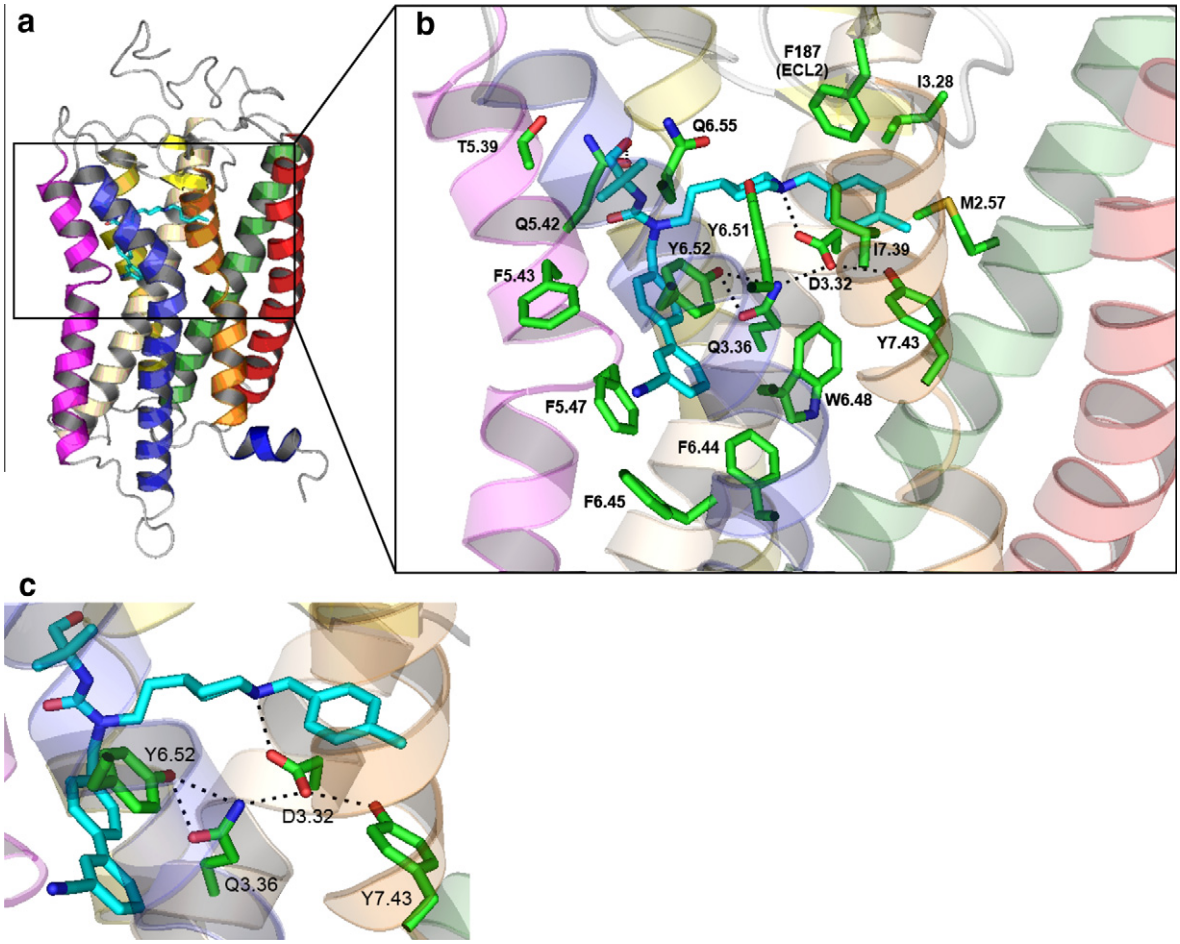

Figure 10. Homology model of the MCHR1 with the antagonist **2t** bound in the binding pocket. Carbon atoms in the antagonist are colored in blue, while those of the receptor are colored in green. Schematic representation (a), closeup of the binding pocket (b) and detail of hydrogen bonds involving Gln3.36(127) (c). Selected residues are denoted using the Ballesteros–Weinstein numbering scheme.[43] Carbon atoms are colored green for the protein and cyan for the ligand; oxygen atoms are colored red, nitrogen atoms blue and sulfur atoms yellow. Atomic interactions within hydrogen bond distance are shown as dashed black lines. The figure was generated with Pymol (DeLano Scintific, Palo Alto, CA, USA).

selectivity for the MCHR1 is observed for compounds **2p–x**, which present one or more hydroxyl groups predicted to bind Gln5.42 or both Gln5.42 and Gln6.55 (Met in HRH3).

These results coincide with the interactions found in our model between polar groups of the antagonists and glutamine residues Gln5.42 and Gln6.55.

2.8. Appearance of a glutamine residue in positions 3.36, 5.42 and/or 6.55 in other GPCR receptors

Afterwards, the appearance of a glutamine (or a similar asparragine) in positions 3.36, 5.42 and 6.55 was checked through the GPCR family. Even if our compounds did not present an interaction with Gln3.36(127), this one was included in the study because it is thought to belong to the binding site of GPCRs and it has been found to interact with some MCHR1 antagonists.[11,18,39,40]

Table 5 shows a list of the GPCR receptors which present a glutamine, or a similar asparragine, in positions 3.36, 5.42 and/or 6.55. The sequence alignment and the GPCR clustering was taken from a previous study by Surgand et al.[12]

As can be observed, the presence of a glutamine in position 3.36 is almost a peculiarity of the MCHR1. Concerning Gln5.42, only some chemokine receptors present a glutamine in that position, and just 7 other receptors belonging to different clusters have an asparragine. Gln6.55 is more conserved through the GPCR family. However, just 7 receptors from the vasopeptides, opiates and purines receptor clusters (apart from MCHR2) present a glutamine in that position, while several others have an asparragine.

All together, we believe that the three glutamine residues and their interactions with ligands could be important for the design of more selective MCHR1 antagonists.

3. Conclusions

In this study, we present a model for the binding of two new series of antagonists to the MCHR1 receptor that is validated using the biological affinity data of the compounds against both MCHR1 and HRH3. Biological data for this second receptor corroborate the role of two glutamines (Gln5.42 and Gln6.55) in the binding of the antagonists. Those glutamine residues are not conserved in most of the GPCR family members.

From our results, the following conclusions emerge: (i) the biphenyl group binds in an aromatic cage formed by residues Phe5.43(213), Phe5.47(217), Phe6.44(265), Phe6.45(266), Trp6.48 (269) and Tyr6.52(273); (ii) the basic amine of the antagonist is involved in an ionic interaction with Asp3.32(123); (iii) the flexibility of the chain joining the two former scaffolds must be enough to allow a good binding of both of them; (iv) the hydroxyl group present in compounds **2p–u** and the urea hydrogen atom present in compounds **1a–e** are predicted to bind residue Gln5.42(212); (v) if one more hydroxyl group is present (compounds **2v–z**), it could bind residue Gln6.55(276); (vi) the absence of these two glutamines in

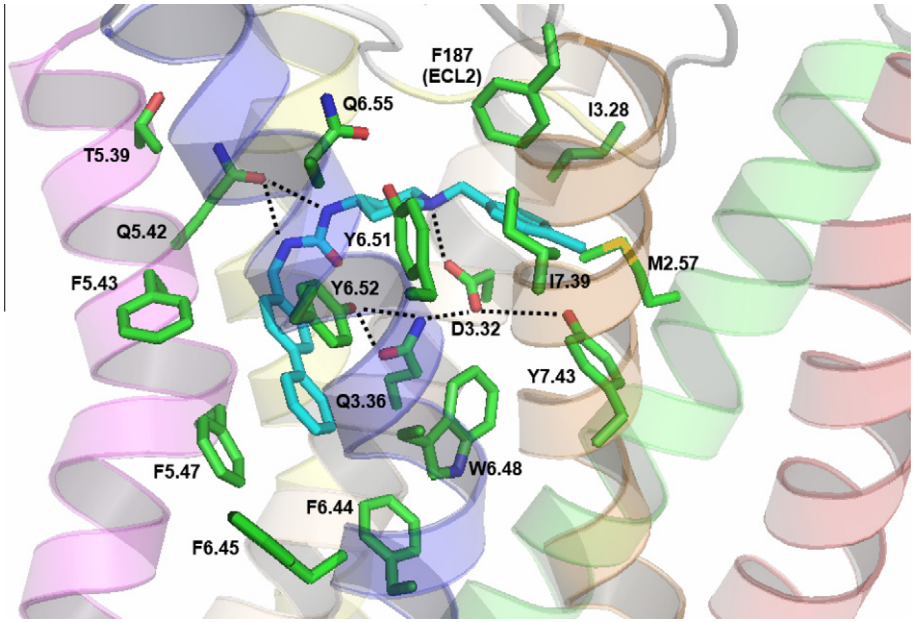

Figure 11. Homology model of the MCHR1 with the antagonist **1e** bound in the binding pocket. Carbon atoms in the antagonist are colored in blue, while those of the receptor are colored in green. Selected residues are denoted using the Ballesteros–Weinstein numbering scheme.[43] Carbon atoms are colored green for the protein and cyan for the ligand; oxygen atoms are colored red, nitrogen atoms are in blue and sulfur atoms are in yellow. Atomic interactions within hydrogen bond distance are shown as dashed black lines. The figure was generated with Pymol (DeLano Scintific, Palo Alto, CA, USA).

	TM1	TM2	TM3	TM4	TM5	TM6	TM7	Sequence homology with MCHR1
	1.35 1.39 1.42 1.46	2.57 2.58 2.61 2.65	3.28 3.29 3.32 3.33 3.36 3.40	4.56 4.60	5.38 5.39 5.42 5.43 5.46	6.44 6.48 6.51 6.52 6.55	7.35 7.39 7.43 7.45	
						★★	★★	
MCHR1	MFIG	MPIM	ITDAQT	SV	FTQFA	FWYYQ	YIYN	
HRH3	LMLT	CIYV	WLDYCA	LA	FLASE	FWYTM	YFWN	23.3%
ADRB2	MMII	VVGI	WTDVVI	TP	YASSS	FWFFN	YNYN	30%
ADRB1	MMII	VVGV	WTDVVI	VP	YASSS	FWFFN	FNYN	26.6%
AA2AR	YEIA	AIAS	IAVLTI	IP	MVNFC	FWLHN	MIHN	20%
OPSD	LMLG	GFTS	EGATGL	CP	FVMFH	FWYAA	MAKA	20%
TRFR	TVIG	AGNS	ITQYIS	YW	IYDFF	FWYRV	LRYN	33.3%
MTLR	VCLG	LPLW	SLGETL	SF	VMVTY	FWFHR	NLYS	20%
GHSR	VCLG	MPLW	FQSETV	SI	VMVSF	FWFHR	NFYS	23.3%
NTR1	VYLG	AMEF	YYRDTA	LM	VINTS	FWYHR	YNYS	20%
NTR2	FYIG	GVEF	YYHEAV	LM	FINVS	YWYHR	YNYS	23.3%
GPR39	LYIG	GMEI	HTFESL	VL	SSGAV	LWNQR	LEYS	16.6%
Q9GZQ4	VYIG	GMEM	KTFECI	FN	IITSF	FWFHR	HGYS	23.3%
Q9HB89	IYIG	GLEM	RTFECV	CN	VVTAF	FWFHR	HGYG	23.3%
MCHR2	LIIG	MPIA	ITDTQS	LV	YTLTT	FAYHQ	YIYS	53.3%

Figure 12. Hotspot residues supposed—from the X-ray structure of bovine rhodopsin bound to retinal- to line the transmembrane binding cavity of ground-state GPCRs.[12] Alignment for MCHR1, HRH3, ADRB2, ADRB1, AA2AR, OPSD and the brain-gut peptides receptors.[12] Sequence identity of each receptor with MCHR1 within the binding site is shown. Residues colored in grey are thought to constitute an aromatic cage for the binding of aromatic groups of the ligand in the amine receptor cluster and our final model.[16,18,37,38] Residues stressed with a black star were found to constitute the aromatic cage in HRH3 by Lorenz et al.[41] MCHR1 glutamines potentially involved in binding of antagonists are stressed in black (Gln3.36, even if not showing interactions with our ligand, has been included). The alignment and clustering of GPCRs was taken from a previous study conducted by Surgand et al., which presented an alignment of 369 nonredundant nonolfatory GPCRs, carried out with the GPCRMOD program.[12] Receptors are named according to their UniProt entry names and amino acid positions identified by the Ballesteros numering scheme.[43] MCHR1: G protein-coupled receptor 24; HRH3: Histamine H3 receptor; ADRB2: β-2 adrenergic receptor; ADRB1: β-1 adrenergic receptor; AA2AR: Adenosine A2a receptor; OPSD: Rhodopsin; TRFR: Thyrotropin-releasing hormone; MTLR: Motilin receptor; GHSR: Growth hormone secretagogue; NTR1: Neurotensin receptor type 1; NTR1: Neurotensin receptor type 2; GPR39: G protein-coupled receptor 39; Q0GZQ4: Neuromedin U receptor 2; Q9HB89: Neuromedin U receptor 1; MCHR2: Melanin-concentrating hormone 2 receptor.

the HRH3 receptor could be the reason why compounds presenting polar groups in the former mentioned positions were found to be selective to our receptor.

In summary, the presence of small polar groups in the antagonists capable of binding Gln5.42(212) and/or Gln6.55(276) appears to be important for their activity towards the MCHR1 and their selectivity against other GPCR members. Moreover, Gln3.36 could also be important for the affinity and selectivity to our receptor.

4. Experimental procedures

4.1. Preliminary homology model building

Sequences from bovine rhodopsin receptor (Swiss-Prot P02699) and human MCHR1 (Swiss-Prot Q99705) were aligned on the basis of conserved residues and generic fingerprints in the TM regions.[29] The backbone structure of the 7TM domains and of the regions of

Table 5
List of GPCRs presenting either a glutamine or an asparragine in position 3.36, 5.42 and/or 6.55, being the corresponding residue position and name shown by an 'X'

GPCR cluster	UniProt entry name	Position 3.36		Position 5.42		Position 6.55	
		Gln3.36	Asp3.36	Gln5.42	Asp5.42	Gln6.55	Asp6.55
Glutamate receptors	TS1R2				X		
Peptides receptors	KISSR				X		
	OX2R						X
	OX1R						X
	GPR10						X
	NPY1R						X
	NPY4R						X
	GASR						X
	CCKAR						X
Melanotonin receptors	GPR22						X
Vasopeptides receptors	V2R					X	
	V1AR					X	
	V1BR					X	
	OXYR					X	
Adenosine receptor s	AA3R						X
	AA1R				X		X
	AA2BR				X		X
	AA2AR				X		X
Amines receptors	5HT2A						X
	5HT2B						X
	5HT2C						X
	DRD1						X
	DRD5						X
	5HT4R						X
	ADRB3						X
	ADRB1						X
	ADRB2						X
	5HT6R						X
Brain-gut peptides receptors	MCHR1	X		X		X	
	MCHR2	X				X	
	NTR1				X		
	NTR2				X		
Chemokines receptors	XCR1			X			
	CXCR3			X			
	CCBP2			X			
	CCR10			X			
	CCR7			X			
	CXCR6			X			
Opiates receptors	R3R1						X
	SSR5	X					X
	SSR2	X					X
	SSR3	X					X
	SSR4					X	
	SSR1					X	
Chemoattractants receptors	CML1						X
Purines receptors	GPR40						X
	PTAFR					X	

The alignment and clustering of GPCRs was taken from a previous study conducted by Surgand et al., which presented an alignment of 369 nonredundant nonolfatory GPCRs, carried out with the GPCRMOD program.[12] Receptors are named according to their UniProt entry names and amino acid positions identified by the Ballesteros numering scheme.[43] TS1R2: Taste receptor TAS1R2; KISSR: G protein-coupled receptor 54; OX2R: Orexin receptor type 2; OX1R: Orexin receptor type 1; GPR10: Prolactin-releasing peptide receptor; NPY1R: Neuropeptide Y receptor type 1; NPY4R: Neuropeptide Y receptor type 4; GASR: Gastrin/cholecystokinin type B receptor; CCKAR: Cholecystokinin type A receptor; GPR22: G protein-coupled receptor 22; V2R: Vasopressin V2 receptor; V1AR: Vasopressin V1a receptor; V1BR: Vasopressin V1b receptor; OXYR: Oxytocin receptor; AA3R: Adenosine A3 receptor; AA1R: Adenosine A1 receptor; AA2BR: Adenosine A2b receptor; AA2AR: Adenosine A2a receptor; 5HT2A: 5-hydroxytryptamine 2A receptor; 5HT2B: 5-hydroxytryptamine 2B receptor; 5HT2C: 5-hydroxytryptamine 2C receptor; DRD1: D1A dopamine receptor; DRD5: D1B (D5) dopamine receptor; 5HT4R: 5-hydroxytryptamine 4 receptor; ADRB3:β-3 adrenergic receptor; ADRB1: β-1 adrenergic receptor; ADRB2: β-2 adrenergic receptor; 5HT6R: 5-hydroxytryptamine 6 receptor; MCHR1: G protein-coupled receptor 24; MCHR2: Melanin-concentrating hormone 2 receptor; NTR1: Neurotensin receptor type 1; NTR2: Neurotensin receptor type 2; XCR1: Chemokine XC receptor 1; CXCR3: C-X-C chemokine receptor type 3; CCBP2: Chemokine binding protein 2; CCR10: C-C chemokine receptor type 10; CCR7: C-Cchemokine receptor type 7; CXCR6: C-X-C chemokine receptor type 6; R3R1: Somatostatin- and angiogenin-like peptide Receptor; SSR5: Somatostatin receptor type 5; SSR2: Somatostatin receptor type 2; SSR3: Somatostatin receptor type 3; SSR4: Somatostatin receptor type 4; SSR1: Somatostatin receptor type 1; CML1: Chemokine receptor-like 1 (ChemR23); GPR40: G protein-coupled receptor 40; PTAFR: Platelet activating factor receptor.

the loops presenting good alignment between both proteins were inherited from the bovine rhodopsin X-ray structure (protein data bank entry 1U19).[19] The side chains corresponding to the MCHR1 sequence were added afterwards. The extra- and intracellular loops were completed using the loop search option in sybyl v7.3 (Tripos associates, St. Louis, MI, USA). A disulfide bridge between Cys116 in TM3 and Cys194 in ECL2, corresponding to the Cys110-Cys187 bridge in rhodopsin,[42] was included in the model. The nomenclature of Ballesteros and Weinstein is used, whereby the most conserved residue in helix X is labelled as X.50.[43]

4.2. Minimization of the preliminary homology model

The resulting structure was energy minimized using the ff99 force field implemented in the AMBER7 molecular dynamics package.[44] Positional restraints were applied to the α-carbons of

all residues except for those that presented disallowed ramachadran conformations, and to the side chains of the residues conserved between both receptors.

4.3. Compound sketching for automated docking

All compounds were sketched using the Sybyl v7.3 molecular modeling software (Tripos associates, St. Louis, MI, USA) and energy minimized with three consecutive optimization algorithms, the steepest descent, conjugate gradient, and quasi-Newton (Broyden, Fletcher, Goldfarb, and Shanno; BFGS) methods, until convergences of 0.05, 0.01 and 0.001 kcal/mol Å, respectively.

4.4. Parameter development for the AMBER force field

ESP charges for compound **2t** were calculated using GAMESS (6-313* basis set). The RESP fit was performed using a two-step procedure described by Bayly et al.[45]

4.5. Molecular dynamics simulation and minimization of the three preliminary ligand–receptor complexes

The three ligand–receptor complexes obtained from the rigid receptor–flexible ligand docking were energy minimized using the ff99 force field implemented in the AMBER7 molecular dynamics package.[44] Positional restraints were applied to the α-carbons of all residues except for those that presented disallowed ramachadran conformations, and to the side chains of those residues conserved between both receptors. The complexes were further submitted to a molecular dynamics simulation lasting 200 ps. Harmonic restraints (100 kcal mol^{-1} $Å^{-2}$) were applied to the α-carbons of the TM domains. The positional restraints that were subsequently applied invariably to all SA runs (see Table 1) were used. Finally, the complexes were once again energy minimized, applying positional restraints to the α-carbons of the TM domains.

4.6. Simulated annealing procedure

20 Runs, AMBER7,[44] in vacuo, heating up to 1500 K in 5 ps and then slowly cooling down to 0 K between 25 ps and 50 ps. Harmonic restraints (100 kcal mol^{-1} $Å^{-2}$) were applied to α-carbons in all SA runs.

4.7. Enthalpy calculation

Ligand–receptor binding enthalpy was estimated as the ligand–receptor interaction enthalpy, where the van der Waals, electrostatic, hydrogen bonding, and torsional energy terms were considered.

4.8. Molecular dynamics simulation

In a first step, the complex was completely solvated in a TIP3P periodic water box and equilibrated for 25 ps at 300 K and under constant pressure conditions, keeping the protein and ligand atoms fixed in their positions. The system was subsequently minimized, applying harmonic restraints on the transmembrane α-carbons. For the molecular dynamics simulation, a water-vacuum-water periodic box was used, following a procedure described in a previous work.[27] The system was heated to 300 K in 2 ps and simulated in NVT conditions for 200 ps while gradually reducing all restraints to zero. Only the distance restraints applied invariably in all the SA runs (see Table 1) were used. This was followed by an unrestrained molecular dynamics simulation lasting 2 ns, using the SHAKE algorithm to constrain the covalent bonds involving hydrogen.[44] The non-bonded residue-based cut-off for both electrostatic and Lennard–Jones interactions was 8 Å. The simulation was carried out using the Sander module implemented in the AMBER7 package.[44]

4.9. MCHR1 binding assays

Binding assays for MCHR1 were performed as described in Galiano et al.[17]

4.10. HRH3 binding assays

Binding assays for HRH3 were performed as described in Cogé et al.[46]

Acknowledgment

We thank Carmen Elizalde# and Rosa Jimenez# for their collaboration in this study.

Supplementary data

Supplementary data associated with this article can be found, in the online version, at doi:10.1016/j.bmc.2010.09.014.

References and notes

1. Abelson, P.; Kennedy, D. *Science* **2004**, *304*, 1413.
2. Bray, G. A.; Bellanger, T. *Endocrine* **2006**, *29*, 109.
3. Neary, M. L.; Goldstone, A. P.; Bloom, S. *Clin. Endocrinol.* **2004**, *60*, 153.
4. (a) Jebb, S. A.; Siervo, M.; Fruehbeck, G.; Goldberg, G. R.; Murgatroyd, P. R.; Prentice, A. M. *Int. J. Obes.* **2006**, *30*, 1160; (b) Seeley, R. J.; Woods, S. C. *Nat. Rev. Neurosci.* **2003**, *4*, 901.
5. Erickson, S. D.; Banner, B.; Berthel, S.; Conde-Knape, K.; Falcioni, F.; Hakimi, I.; Hennessy, B.; Kester, R. F.; Kim, K.; Ma, C.; McComas, W.; Mennona, F.; Mischke, S.; Orzechowski, L.; Qian, Y.; Salari, H.; Tengi, J.; Thakkar, K.; Taub, R.; Tilley, J. W.; Wang, H. *Bioorg. Med. Chem. Lett.* **2008**, *18*, 1402.
6. Bittencourt, J. C.; Presse, F.; Arias, C.; Peto, C.; Vaughan, J.; Nahon, J. L. *J. Comp. Neurol.* **1992**, *319*, 218.
7. Rossi, M.; Choi, S. J.; O'Shea, D.; Miyoshi, M. A.; Ghatei, S. R.; Bloom, S. R. *Endocrinology* **1997**, *138*, 351.
8. Shimada, M.; Tritos, N. A.; Lowell, B. B.; Flier, J. S.; Maratos-Flier, E. *Nature* **1998**, *396*, 670.
9. Ludwig, D. S.; Tritos, N. A.; Mastaitis, J. W.; Kulkarni, R.; Kokkotou, E.; Elmquist, J., et al *J. Clin. Invest.* **2001**, *107*, 379.
10. Borowsky, B.; Durkin, M. M.; Ogozalek, K.; Marzabadi, M. R.; DeLeon, J.; Lagu, B., et al *Nat. Med.* **2002**, *8*, 825.
11. Chen, Y.; Hu, C.; Hsu, C. K.; Zhang, O.; Bi, C.; Asnicar, M., et al *Endocrinology* **2002**, *143*, 2469.
12. Surgand, J.-S.; Rodrigo, J.; Kellenberger, E.; Rognan, D. *Proteins* **2006**, *62*, 509.
13. Dixon, R. A. F.; Sigal, I. S.; Strader, C. D. *Cold Spring Harb. Symp. Quant. Biol.* **1988**, *53*, 487.
14. Strader, C. D.; Sigal, I. S.; Dixon, R. A. *Trends Pharmacol. Sci.* **1989**, 26.
15. Vitale, R. M.; Pedone, C.; De Benedetti, P. G.; Fanelli, F. *Proteins* **2004**, *56*, 430.
16. Ulven, T.; Frimurer, T. M.; Receveur, J. M.; Little, P. B.; Rist, O.; Norregaard, P. K.; Hogberg, T. *J. Med. Chem.* **2005**, *48*, 5684.
17. Galiano, S.; Ceras, J.; Cirauqui, N.; Perez, S.; Juanenea, L.; Rivera, G.; Aldana, I.; Monge, A. *Bioorg. Med. Chem.* **2007**, *15*, 3896.
18. Cavasotto, C. N.; Orry, A. J. W.; Murgolo, N. J.; Czarniecki, M. F.; Kocsi, S. A.; Hawes, B. E.; O'Neill, K. A.; Hine, H.; Burton, M. S.; Voigt, J. H.; Abagyan, R. A.; Bayne, M. L.; Monsma, F. J. *J. Med. Chem.* **2008**, *51*, 581.
19. Okada, T.; Sugihara, M.; Bondar, A. N.; Elstner, M.; Entel, P.; Buss, V. *J. Mol. Biol.* **2004**, *342*, 571.
20. Park, J. H.; Scheerer, P.; Hofmann, K. P.; Choe, H.-W.; Ernst, O. P. *Nature* **2008**, *454*, 183.
21. Scheerer, P.; Park, J. H.; Hildebrand, P. W.; Kim, Y. J.; Krauss, N.; Choe, H.-W.; Hofmann, K. P.; Ernst, O. P. *Nature* **2008**, *455*, 497.
22. Cheredov, V.; Rosenbaum, D. M.; Hanson, M. A.; Rasmussen, S. G.; Thian, F. S.; Kobilka, T. S.; Choi, H. J.; Kuhn, P.; Weis, W. I.; Kobilka, B. K.; Stevens, R. C. *Science* **2007**, *318*, 1258.
23. Warne, A.; Serrano-Vega, M. J.; Baker, J. G.; Moukhametzianov, R.; Edwards, P. C.; Henderson, R.; Leslie, A. G. W.; Tate, C. G.; Schertler, G. F. X. *Nature* **2008**, *454*, 486.
24. Jaakola, V. P.; Griffith, M. T.; Hanson, M. A.; Cherezov, V.; Chien, E. Y.; Lane, J. R.; Ijzerman, A. P.; Stevens, R. C. *Science* **2008**, *322*, 1211.
25. Kratochwil, N. A.; Malherbe, P.; Lindemann, L.; Ebeling, M.; Hoener, M. C.; Muehlemann, A.; Porter, R. H. P.; Stahl, M.; Gerber, P. R. *J. Chem. Inf. Model.* **2005**, *45*, 1324.
26. Jain, A. N. *J. Med. Chem.* **2003**, *46*, 499.
27. Ter Laak, A. M.; Kühne, R. *Receptors Channels* **1999**, *6*, 295.

28. http://www.soe.ucsc.edu/research/compbio/HMM-apps/T02-query.html.
29. Ballesteros, J. A.; Shi, L.; Javitch, J. A. *Mol. Pharmacol.* **2001**, *60*, 1.
30. Klabunde, T.; Hesser, G. *Chembiochem* **2002**, *3*, 928.
31. Okada, T.; Fujiyoshi, Y.; Silow, M.; Navarro, J.; Landau, E. M.; Shichida, Y. *Proc. Natl. Acad. Sci. U.S.A.* **2002**, *99*, 5982.
32. Ballesteros, J. A.; Jensen, A. D.; Liapakis, G.; Rasmussen, S. G.; Shi, L.; Gether, U.; Javitch, J. A. *Biol. Chem.* **2001**, *276*, 29171.
33. Palczewski, K.; Kumasa, T.; Hori, T.; Behnke, C. A.; Motoshima, H.; Fox, B. A.; Le Trong, I.; Teller, D. C.; Okada, T.; Stenkamp, R. E.; Yamamoto, M.; Miyano, M. *Science* **2000**, *289*, 739.
34. Labbe-Jullie, C.; Barroso, S.; Nicolas-Eteve, D.; Reversat, J. L.; Botto, J. M.; Mazella, J.; Bernassau, J. M., et al *J. Biol. Chem.* **1998**, *273*, 16351.
35. Tavares, F. X.; Al-Barazanji, K. A.; Bigham, E. C.; Bishop, M. J.; Britt, C. S.; Carlton, D. L.; Feldman, P. L.; Goetz, A. S.; Grizzle, M. K.; Guo, Y. C.; Handlon, A. L.; Hertzog, D. L.; Ignar, D. M.; Lang, D. G.; Ott, R. J.; Peat, A. J.; Zhou, H.-Q. *J. Med. Chem.* **2006**, *49*, 7095.
36. Cho, W.; Taylor, L. P.; Mansour, A.; Akil, H. *J. Neurochem.* **1995**, *65*, 2105.
37. Javitch, J. A.; Ballesteros, J. A.; Weinstein, H.; Chen, J. *Biochemistry* **1998**, *37*, 998.
38. Kiss, R.; Kovári, Z.; Keserű, G. M. *Eur. J. Med. Chem.* **2004**, *39*, 959.
39. Clark, D. E.; Higgs, C.; Wren, S. P.; Dyke, H. J.; Wong, M.; Norman, D.; Lockery, P. M.; Roach, A. G. *J. Med. Chem.* **2004**, *47*, 3962.
40. Giordanetto, F.; Karlsson, O.; Lindberg, J.; Larsson, L.-O.; Linusson, A.; Evertsson, E.; Morgan, D. G. A.; Inghardt, T. *Bioorg. Med. Chem. Lett.* **2007**, *17*, 4232.
41. Lorenzi, S.; Mor, M.; Bordi, F.; Rivara, S.; Rivara, M.; Morini, G.; Bertoni, S.; Ballabeni, V.; Barocelli, E.; Plazzi, P. V. *Bioorg. Med. Chem.* **2005**, *13*, 5647.
42. Davidson, J. S.; Assefa, D.; Pawson, A.; Davies, P.; Hapgood, J.; Becker, I.; Flanagan, C.; Roeske, R.; Millar, R. *Biochemistry* **1997**, *36*, 12881.
43. Ballesteros, J.; Weinstein, H. *Methods Neurosci.* **1995**, *25*, 366.
44. Case, D. A.; Pearlman, D. A.; Caldwell, J. W.; Cheatham, T. E., III; Wang, J.; Ross, W. S.; Simmerling, C. L.; Darden, T. A.; Merz, K. M.; Stanton, R. V.; Cheng, A. L.; Vincent, J. J.; Crowley, M.; Tsui, V.; Gohlke, H.; Radmer, R. J.; Duan, Y.; Pitera, J.; Massova, I.; Seibel, G. L.; Singh, U. C.; Weiner, P. K.; Kollman, P. A. *AMBER 7*; University of California: San Francisco, 2002.
45. Bayly, C. I.; Cieplak, P.; Cornell, W. D.; Kollman, P. A. *J. Phys. Chem.* **1993**, *97*, 10269.
46. Cogé, F.; Guénin, S.-P.; Audinot, V.; Renouard-Try, V.; Beauverger, P.; Macia, C.; Ouvry, C.; Nagel, N.; Boutin, J. A.; Galizzi, J.-P. *Biochem. J.* **2001**, *355*, 279.
47. Ter Laak, A. M.; Timmerman, H.; Leurs, R.; Nedekoorn, P. H. J.; Smit, M. J.; Donné-Op den Kelder, G. M. *J. Comput. Aided Mol. Des.* **1995**, *9*, 319–330.
48. Hövelmann, S.; Hoffmann, S. H.; Kühne, R.; Ter Laak, A. M.; Reilander, H.; Beckers, T. *Endocr. Rev.* **1997**, *18*, 180.
49. Marco, E.; Foucaud, M.; Langer, I.; Escrieut, C.; Tikhonova, I. G.; Fourmy, D. *J. Biol. Chem.* **2007**, *282*, 28779.
50. Pogozheva, I. D.; Przydzial, M. J.; Mosberg, H. I. *AAPS J.* **2005**, *7*, E434.
51. Clark, A. M.; Labute, P.; Santavy, M. *J. Chem. Inf. Model.* **2006**, *46*, 1107.